Muonic Atoms and the Radial Shape of the Nuclear Charge Distribution*

KENNETH W. FORD† AND JOHN G. WILLS‡
University of California, Los Alamos Scientific Laboratory, Los Alamos, New Mexico 87544
(Received 10 March 1969)

We find, for a rather broad set of two-, three-, and four-parameter charge-density functions, that a particular muonic-atom transition energy determines a particular moment of the nuclear charge density, $\langle r^k \rangle$. The exponent k depends on the atomic number Z and on the quantum numbers of the pair of states in question, but it depends only very weakly on the mathematical form of the charge-density function. Consequently, an almost model-independent analysis of muonic-atom energies is possible. This analysis is facilitated by introduction of the equivalent radius R_k, defined by $R_k=[\frac{1}{3}(k+3)\langle r^k \rangle]^{1/k}$. For $Z=82$, a range of moments from $k=0.08$ to $k=4.80$ is provided by available data. The $2p_{1/2}\rightarrow 1s_{1/2}$ transition in lead, for example, measures the $k=0.80$ moment and determines $R_{0.8}\cong 7.013-1.49(E-5.788)$ F, where E is the transition energy in MeV. For this transition, as well a for several others, k is approximately a linear function of Z.

I. INTRODUCTION

THE measurement of the $2p_{3/2}\rightarrow 1s_{1/2}$ energy for a particular muonic atom determines, of course, only a single parameter of the nuclear charge distribution. Since the earliest days of analyzing muonic x-ray energies, workers have recognized[1] that different transitions determine different parameters, so that, in principle, energy measurements for a number of different transitions in a given atom might provide information about the radial shape of the nuclear charge density. [By radial shape, we mean simply the form of the charge-density function $\rho(r)$.] However, it has not been clear exactly what nuclear parameter is determined by a particular transition, except in the low-Z limit, where nonrelativistic perturbation theory shows that level shifts are proportional to even moments of the charge density.[2] In this limit, for instance, the $2p\rightarrow 1s$ transitions measure the mean square radius $\langle r^2 \rangle$. One occasionally hears or reads that the same is true for heavy atoms. This is not the case. Even for Z as low as 6, the $2p\rightarrow 1s$ transitions do not determine exactly the mean square radius.

In the work described here, we set out to answer the following question: Exactly what parameter of the nuclear charge distribution is determined by each transition energy? We have found that, with a remarkable degree of model independence, most transitions (or energy differences, such as $2p_{3/2}-2p_{1/2}$) determine specific moments of the charge density $\langle r^k \rangle$. For each transition, the exponent k is an even integer at $Z=0$, and decreases smoothly—in some cases, almost linearly—with increasing Z. These results are based mostly on a trial-and-error procedure using exact numerical calculation. The general trend of k can be understood analytically, but the fact that it should vary linearly with Z and the fact that the moment determination at large Z should be so nearly model-independent are facts without a good theoretical foundation at present.

It has become customary to define an equivalent uniform radius (which we here call R_2) as the radius of a uniformly charged sphere with the same mean square radius as a particular charge distribution of interest. To discuss the results of our work, it is convenient to define an equivalent radius more generally for all moments $\langle r^k \rangle$. The definition is

$$R_k=[\tfrac{1}{3}(k+3)\langle r^k \rangle]^{1/k}. \quad (1)$$

Then we can say that a measured energy difference for a particular muonic atom determines k and R_k. A set of different transitions at given Z determine a set of equivalent radii R_k, which then delimit the possible radial shapes of the charge distribution. As a result of numerical calculations, a set of approximate formulas of the following form can be developed:

$$R_k=R_k^{(0)}-C(E-E^{(0)}). \quad (2)$$

Here $E^{(0)}$ is a standard transition energy, chosen to be nearly equal to a measured value E. The equivalent radius $R_k^{(0)}$ is that determined by $E^{(0)}$; the equivalent radius R_k is that determined by E. The energy-dependence coefficient C, like k, $R_k^{(0)}$, and $E^{(0)}$, depends on Z and the quantum numbers of the pair of levels in question. However, the quantities k and C depend only weakly on the functional form of the charge density $\rho(r)$, and they do not vary significantly as the energy E is artificially varied over a range greater than the actual uncertainty of E.

* The major part of this work was performed at the Los Alamos Scientific Laboratory under the auspices of the U.S. Atomic Energy Commission. Partial support came also from the National Science Foundation and from the University of California, Irvine.
† Permanent address: Physics Department, University of California, Irvine, Calif. 92664.
‡ Permanent address: Physics Department, Indiana University, Bloomington, Ind. 47401.
[1] David L. Hill and Kenneth W. Ford, Phys. Rev. **94**, 1617 (1954).
[2] An accurate version of perturbation theory for energy shifts in heavy muonic atoms has been developed recently by H. A. Bethe and J. W. Negele, Nucl. Phys. **A117**, 575 (1968).

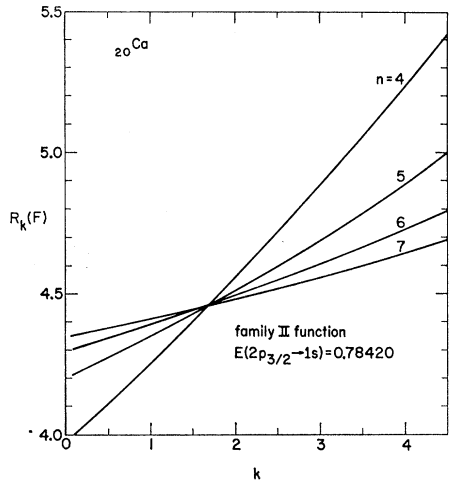

FIG. 1. Equivalent-radius functions for several different Family-II charge-density functions in calcium, all yielding the same $2p_{3/2}\rightarrow 1s_{1/2}$ transition energy.

II. FAMILIES OF CHARGE-DISTRIBUTION FUNCTIONS

To study the model dependence of our results, we carried out calculations with all of the following functional forms.

Family II (three-parameter)

$$\rho(r)=\rho_0[1+w(r/R)^2][1-\tfrac{1}{2}e^{-n(R-r)/R}], \quad r<R$$
$$=\rho_0(1+w)\tfrac{1}{2}e^{-n(r-R)/R}, \quad r>R \qquad (3)$$

Fermi (three-parameter)

$$\rho(r)=\rho_0[1+w(r/R)^2](1+e^{(r-R)/a})^{-1}, \quad r<R$$
$$=\rho_0(1+w)(1+e^{(r-R)/a})^{-1}, \quad r>R \qquad (4)$$

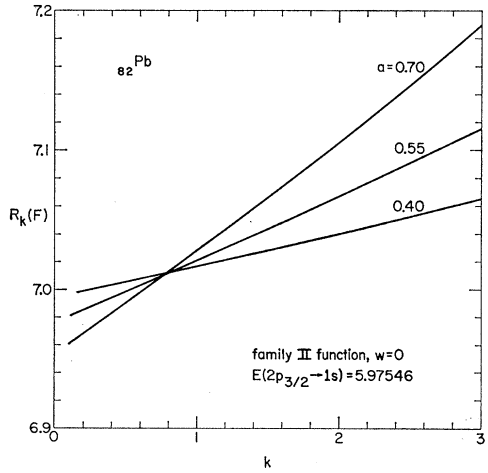

FIG. 2. Graphical determination of critical k value and equivalent radius for the $2p_{3/2}\rightarrow 1s_{1/2}$ transition in lead. Same as Fig. 1 except for change of atomic number and change of transition energy. The curves are labeled by $a=R/n$.

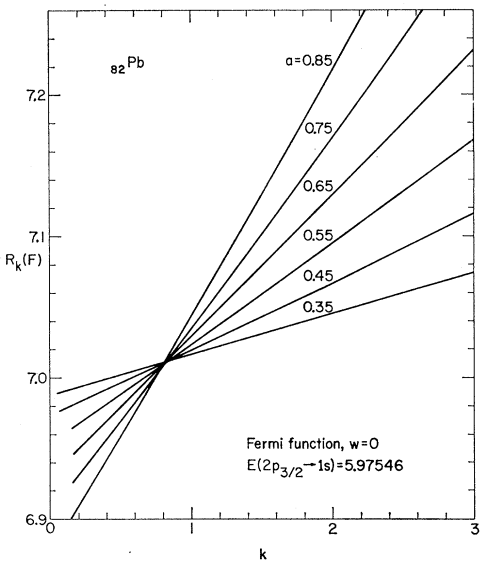

FIG. 3. Graphical determination of critical k value and equivalent radius for the $2p_{3/2}\rightarrow 1s_{1/2}$ transition in lead. Same as Fig. 2 except for change of functional form of charge-density function.

Bethe[3] *(two-parameter)*

$$\rho(r)=\rho_0(1-e^{(r-R)/a})^2, \quad r<R$$
$$=0, \quad r>R \qquad (5)$$

Bethe-Elton[3] *(four-parameter)*

$$\rho(r)=\rho_0[1+w(r/R)^2](1-\tfrac{1}{2}e^{(r-R)/a})^2, \quad r<R$$
$$=\rho_0(1+w)\tfrac{1}{4}e^{-\gamma(r-R)}, \quad r>R. \qquad (6)$$

Notice that the parabolic wine-bottle term is carried

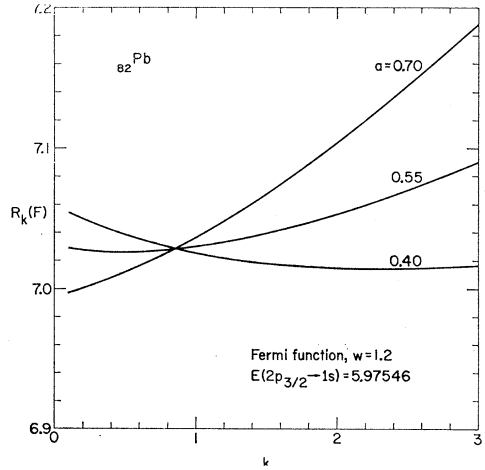

FIG. 4. Graphical determination of critical k value and equivalent radius for the $2p_{3/2}\rightarrow 1s_{1/2}$ transition in lead. Same as Figs. 2 and 3 except for change of functional form of charge-density function.

[3] H. A. Bethe and L. R. B. Elton, Phys. Rev. Letters **20**, 745 (1968).

only to $r=R$, and replaced by the constant factor $1+w$ for $r>R$. Except when explicitly stated otherwise, the parameter w is set equal to zero. The Bethe function is unrealistic in having $\rho=0$ beyond some radius R. Both the Family-II and Fermi functions, despite their three parameters, are limited in that the surface thickness (e.g., the 90–10% distance) is directly proportional to the falloff distance in the tail of the distribution. With its fourth parameter, the Bethe-Elton function can provide for independent variation of the surface thickness and the falloff distance at large r. We also made a few calculations with a four-parameter Fermi function, one in which an exponential tail of arbitrary half-distance replaced the second line of Eq. (4) in the region where $\rho<0.1\rho_0$. This change of the function at large r produced no significant effects of interest.

A given charge density $\rho(r)$ can be completely characterized by its equivalent radius function $R_k(k)$. We call attention to some features of curves of R_k versus k. For a uniform charge density, the R_k curve is a straight horizontal line. As the surface thickness grows, the R_k curve swings around to greater positive slope (see Figs. 1–3). For the Fermi function with $w=0$, the R_k curve is nearly a straight line over the range $0\leq k\lesssim 4$ (see Fig. 3). With a central depression in the charge density (positive w), the R_k curve takes on greater positive curvature (see Fig. 4). These qualitative features are useful in analyzing the equivalent radii determined by experiment.

The limit of R_k as $k\to 0(R_0)$ is not simply proportional to the normalization integral $\langle r^0\rangle$. Rather R_0 is a meaningful radial parameter. It may be expressed in terms of the potential by

$$R_0=A\exp\left[\frac{4}{3}-\int_0^A\varphi(r)\,dr\right], \qquad (7)$$

where $\varphi(r)$ is the electrostatic potential for the charge density in question, normalized so that $\varphi(r)=r^{-1}$ for $r\geq A$. The parameter A must be chosen large enough so that the charge density $\rho(A)$ is sensibly zero. Then R_0 is independent of A.

A. Numerical Calculation

Using methods similar to those employed in earlier work,[4,5] we integrated the radial Dirac equations to obtain eigenvalues and eigenfunctions of the muon in the field of a static spherically symmetric nucleus. With these eigenfunctions, we calculated the vacuum-polarization correction numerically to lowest order in $r/\lambda\!\!\!^{-}_e$,[4] where $\lambda\!\!\!^{-}_e=\hbar/m_ec=386$ F. The next term in such an expansion of the vacuum-polarization potential adds the same binding energy, Z Ry, to all levels, and has no effect on energy differences. The third term, which is repulsive, we estimated by hand. It amounts to about 0.07 keV for f states in lead. McKee[6] has developed a better method of calculating the vacuum-polarization energy.

In these calculations we chose for the muon mass[7]

$$m=206.767m_e=105.659\text{ MeV},$$

and we used the nonrelativistic reduced mass of the system.

III. ANALYSIS OF $2p_{3/2}\to 1s_{1/2}$ TRANSITIONS

Figure 1 illustrates the method of finding k and R_k. The standard energy for the $2p_{3/2}\to 1s_{1/2}$ transition in calcium is chosen to be 0.78420 MeV.[8] For each of several surface thickness parameters n of the Family-II function, the radial parameter R is adjusted until the calculated transition energy is exactly the standard energy. For the different functions $\rho(r)$, all yielding the same transition energy, the R_k curves are plotted. In this example, the curves intersect at a point $k=1.70$, $R_k=4.458$. This is the common feature of the functions whose surface thicknesses span a factor of 2. Model independence is checked by repeating the calculations for other functional forms of $\rho(r)$. Results for the $2p_{3/2}\to 1s_{1/2}$ transition in $_{20}$Ca are given in Table I. Except for the Bethe function, which lacks an exponential tail, consistency is good. The transition is measuring approximately the $k=1.72$ moment instead of the $k=2.00$ moment predicted by nonrelativistic perturbation theory. Vacuum-polarization corrections are included in these calculations, but other corrections are not.

Figures 2–4 show the analogous results for the $2p_{3/2}\to 1s_{1/2}$ transition in $_{82}$Pb, with the standard energy chosen to be 5.97546 MeV.[9–11] Comparison of Figs. 1 and 2 shows the effect of changing Z. For $Z=20$ the curves intersect at $k=1.70$; for $Z=82$, they intersect at $k=0.80$. For the Fermi function, the intersection

[4] K. W. Ford and J. G. Wills, Nucl. Phys. **35**, 295 (1962).
[5] K. W. Ford, V. W. Hughes, and J. G. Wills, Phys. Rev. **129**, 194 (1963).
[6] R. J. McKee, Enrico Fermi Institute for Nuclear Studies Report No. 68-39, 1968 (unpublished).
[7] N. Barash-Schmidt, A. Barbaro-Galtieri, L. R. Price, M. Roos, A. H. Rosenfeld, P. Söding, and C. G. Wohl, University of California Lawrence Radiation Laboratory Report No. UCRL-8030, 1968 (unpublished).
[8] This is close to the experimental value reported by H. L. Acker, G. Backenstoss, C. Daum, J. C. Sens, and S. A. DeWit, Nucl. Phys. **87**, 1 (1966).
[9] Experimental energies for lead are given in Ref. 8, and in several other recent publications, including H. L. Anderson, R. J. McKee, C. K. Hargrove, and E. P. Hincks, Phys. Rev. Letters **16**, 434 (1966); and R. J. Powers, Phys. Rev. **169**, 1 (1968).
[10] The most extensive and most precise data on transition energies in lead isotopes are given by H. L. Anderson, C. K. Hargrove, E. P. Hincks, J. D. McAndrew, R. J. McKee, R. D. Barton, and D. Kessler, Phys. Rev. (to be published) (1969). Part of this work appeared earlier in H. L. Anderson's contribution to Proceedings of the International Conference on Electromagnetic Sizes of Nuclei, Ottawa, Canada, 1967 (unpublished), and in Ref. 11.
[11] H. L. Anderson, C. K. Hargrove, E. P. Hincks, J. D. McAndrew, R. J. McKee, and D. Kessler, Phys. Rev. Letters **22**, 221 (1969).

TABLE I. Values of k and R_k determined for the $2p_{3/2}\rightarrow 1s_{1/2}$ transition in $_{20}$Ca, using several functional forms of $\rho(r)$.

Charge-density function	k	R_k for $E=0.7842$ MeV
Family II ($w=0$)	1.70	4.458
Fermi ($w=0$)	1.72	4.460
Fermi ($w=0.6$)	1.72	4.460
Fermi ($w=1.2$)	1.72	4.462
Bethe	1.85	4.465

point for Pb is at $k=0.83$ (Fig. 3). In both Figs. 2 and 3, the critical equivalent radius is $R_k=7.012$ F. The effect of a large central depression ($w=1.2$) is shown in Fig. 4. There the intersection point is at $k=0.85$, $R_k=7.028$.

The results of such determinations of moments are presented as a function of atomic number in Fig. 5. Remarkably, the critical exponent k diminishes linearly with increasing Z, with value $k=2$ at $Z=0$, and with $dk/dZ=-0.0145$. The critical values of k as determined using the Fermi function are presented in Table II, together with standard energies and equivalent radii for these energies.

For low Z, the $2p$-state energy shift is negligible compared with the $1s$-state energy shift, and the $1s$ binding energy measures the same nuclear parameter as does the $2p\rightarrow 1s$ energy. For large Z, the $2p$-state energy shift is, relative to the $1s$-state energy shift, small but not negligible. For $Z=82$, we find (using the Fermi function) that the $1s$ binding energy is sensitive to the $k=1.03$ moment of the nuclear charge density. Although the $1s$ binding energy is not directly measurable, it plays an independent role in the isomer shift. For this phenomenon in heavy atoms, the relevant k value is slightly larger than the value appropriate for the $2p\rightarrow 1s$ transitions.

A. Model Dependence

Table I and Fig. 5 provide some evidence on the model dependence of our results. Further evidence is provided in Tables III and IV, whose data still apply only to the single $2p_{3/2}\rightarrow 1s_{1/2}$ transition. Different models yield k values consistent within ± 0.02, with the notable exception of the Bethe function and the Bethe-Elton function with fixed γ. These two functions yield k values larger than the others by as much as 0.2. However, each of these is unrealistic in an important way. The Bethe function goes precisely to zero at $r=R$. The Bethe-Elton function has discontinuous slope at $r=R$ if γ is held fixed and only R and a are varied. If we impose the requirement of continuous slope on the Bethe-Elton function, and vary R, a, and γ to maintain this condition (see the last column of Table III), it yields a k value close to the values found for other models. We conclude that, for realistic models, including a wide range of variation of parameters, k is determined to within ± 0.02.

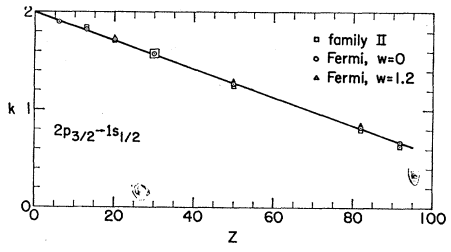

FIG. 5. Critical values of k as a function of atomic number for the $2p_{3/2}\rightarrow 1s_{1/2}$ transition.

For the realistic models without a central charge depression ($w=0$), the R_k values are determined to within about ± 0.002 F. As w grows to 0.6 and then to 1.2, the values of R_k grow slightly, by as much as 0.016 F for $Z=82$ (less for lower Z). Considering that $w=1.2$ is an unrealistically large value of w, this amounts to a very weak model dependence. However, it is enough to require consideration if precision fitting of data is the goal.

TABLE II. Values of k and R_k determined for $2p_{3/2}\rightarrow 1s_{1/2}$ transitions in various elements, using the Fermi function for analysis.

Atomic No. Z	Standard energy $2p_{3/2}\rightarrow 1s_{1/2}$ (MeV)	k	R_k (F)
6	0.0751760	1.90	3.480
13	0.346168	1.82	4.074
20	0.78421	1.72	4.460
30	1.60134	1.57	5.046
50	3.45542	1.27	5.949
82	5.97546	0.83	7.012
92	6.55446	0.67	7.313

IV. ANALYSIS OF OTHER ENERGY DIFFERENCES

We find specific moments of the charge density to be determined by the circular-orbit transitions, $4f\rightarrow 3d$, $3d\rightarrow 2p$, and $2p\rightarrow 1s$; by the doublet p and doublet d splittings; and by the $3p_{3/2}\rightarrow 2s_{1/2}$ transition. Among all the energy differences examined, only the $2s_{1/2}\rightarrow 2p_{1/2}$ transition in Pb failed to show sensitivity to a single moment. A moment determination for the doublet p splitting in Pb is shown, for example, in Fig. 6. Here $k=1.22$, $R_k=7.040$ F. According to relativistic perturbation theory, k should be equal to 2, since the small component of the $p_{1/2}$ wave function behaves like an s-state wave function. Another example is shown in Fig. 7. The $3d_{3/2}\rightarrow 2p_{3/2}$ transition, which measures the $k=4.0$ moment at low Z, measures the $k=2.76$ moment at $Z=82$. In Fig. 7, the intersection points occur at $k=2.76$, $R_k=7.152$ for $w=0$, and $k=2.77$, $R_k=7.161$ for $w=1.2$.

A summary of critical k-values determined using the Fermi function ($w=0$) is tabulated in Table V and

TABLE III. Evidence of model dependence. Values of k determined for the $2p_{3/2}\rightarrow 1s_{1/2}$ transitions in various atoms, using a variety of nuclear charge density models.

		Values of k					
Z	Family II	Fermi $w=0$	Fermi $w=0.6$	Fermi $w=1.2$	Bethe	Bethe[a]-Elton fixed γ	Bethe[b]-Elton variable γ
6		1.90					
13	1.84	1.82			1.86		
20	1.70	1.72	1.72	1.72	1.85	1.85	
30	1.57	1.57					
50	1.25	1.27	1.30	1.28	1.43	1.45	
82	0.80	0.83	0.84	0.85	1.00	1.00	0.85
92	0.63	0.67			0.87		

[a] $w=0$, $\gamma=1.8$ fixed; a and R variable.

[b] $w=0$ fixed; a, R, and γ varied to maintain continuous slope at $r=R$.

TABLE IV. Evidence of model dependence. Values of R_k corresponding to the k values of Table III.

		Values of R_k in fermis					
Z	Family II	Fermi $w=0$	Fermi $w=0.6$	Fermi $w=1.2$	Bethe	Bethe-Elton fixed γ	Bethe-Elton variable γ
6		3.480					
13	4.079	4.074			4.077		
20	4.458	4.460	4.460	4.462	4.465	4.472	
30	5.049	5.046					
50	5.951	5.949	5.955	5.959	5.953	5.962	
82	7.012	7.012	7.022	7.028	7.014	7.020	7.010
92	7.313	7.313			7.317		

TABLE V. Critical values of k determined for various transitions and various atomic numbers using the Fermi function for analysis.

	Atomic No., Z						
Energy difference	6	13	20	30	50	82	92
$2p_{1/2}\rightarrow 1s_{1/2}$						0.80	
$2p_{3/2}\rightarrow 1s_{1/2}$	1.90	1.82	1.72	1.57	1.27	0.83	0.67
$2p_{3/2}$-$2p_{1/2}$			1.95[a]	1.87	1.71	1.22	1.06
$3d_{3/2}\rightarrow 2p_{1/2}$						2.29	
$3d_{5/2}\rightarrow 2p_{3/2}$				3.62	3.25	2.76	2.61
$3d_{3/2}\rightarrow 2p_{3/2}$						2.76	
$3d_{5/2}$-$3d_{3/2}$						3.25	
$4f_{5/2}\rightarrow 3d_{3/2}$						4.06	
$4f_{7/2}\rightarrow 3d_{5/2}$						4.80	4.65
$3p_{3/2}\rightarrow 2s_{1/2}$						0.08	
$2s_{1/2}\rightarrow 2p_{1/2}$						none	
$1s_{1/2}$ binding						1.03	

[a] This value is uncertain by about ± 0.05 because of inaccuracy in numerical computation.

TABLE VI. Standard energies and corresponding equivalent radii for selected elements, using the Fermi function for analysis, with k values shown in Table V.

Quantum Nos.		Standard energies $E^{(0)}$ (keV) and equivalent radii $R_k^{(0)}$ (F)					
		$Z=6$	$Z=13$	$Z=20$	$Z=30$	$Z=50$	$Z=92$
$2p_{3/2}\rightarrow 1s_{1/2}$	$E^{(0)}$	75.176	346.17	784.21	1601.34	3455.42	6554.30
	$R_k^{(0)}$	3.480	4.074	4.460	5.046	5.949	7.313
$2p_{3/2}$-$2p_{1/2}$	$E^{(0)}$			1.4814	7.1889	45.594	235.03
	$R_k^{(0)}$			4.48	5.076	5.987	7.339
$3d_{5/2}\rightarrow 2p_{3/2}$	$E^{(0)}$				354.13	982.06	3039.15
	$R_k^{(0)}$				5.260	6.120	7.447
$4f_{7/2}\rightarrow 3d_{5/2}$	$E^{(0)}$						1184.07
	$R_k^{(0)}$						7.592

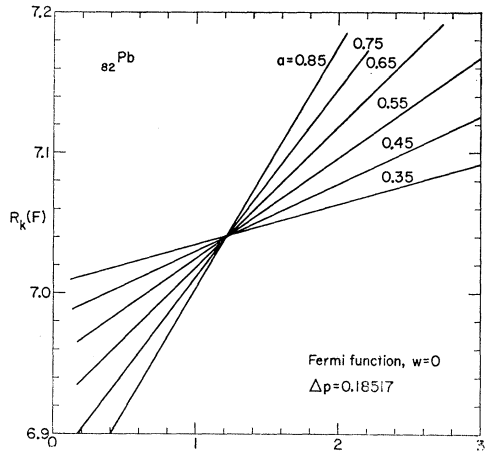

FIG. 6. Graphical determination of critical k value and equivalent radius for the doublet p splitting in lead.

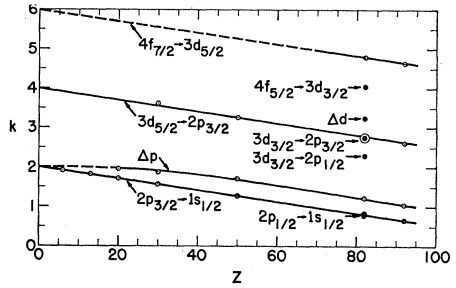

FIG. 8. Critical values of k as a function of atomic number for various transitions and energy differences; the Fermi function was used for the analysis.

illustrated in Fig. 8. Notice that the points for the $4f_{7/2}\rightarrow 3d_{5/2}$, the $3d_{5/2}\rightarrow 2p_{3/2}$, and the $2p_{3/2}\rightarrow 1s_{1/2}$ transitions are consistent with linear functions $k(Z)$, all of the same slope. Because of lack of sensitivity to nuclear radius, the $4f\rightarrow 3d$ transitions cannot be studied at low and intermediate values of Z. As indicated by the solid dots in Fig. 8, some energy differences were studied only at $Z=82$. The standard energies and corresponding equivalent radii found for elements other than lead are summarized in Table VI. For these elements, we did not pursue the numerical calculations far enough to determine the energy dependence coefficients C of Eq. (2).

V. DETAILED ANALYSIS FOR LEAD

A. Energy Dependence of Effective Radii

For $Z=82$, we have selected standard energies close to the experimental energies due to Anderson *et al.*,[10] and, for each of eight transitions and two doublet splittings, we have found the equivalent radii $R_k^{(0)}$ and the energy dependence coefficients C of Eq. (2).

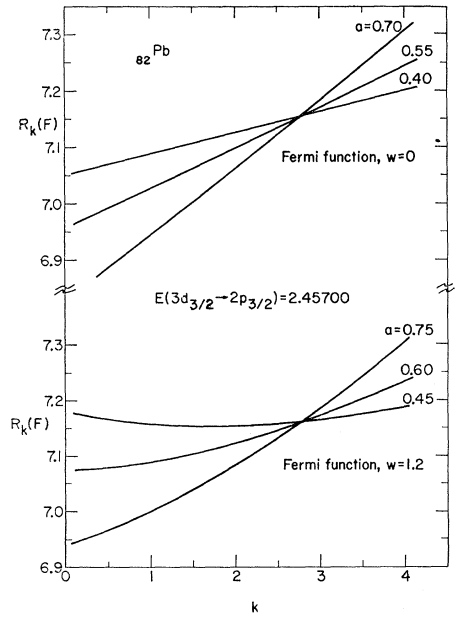

FIG. 7. Graphical determination of critical k value and equivalent radius for the $3d_{3/2}\rightarrow 2p_{3/2}$ transition in lead, for charge-density functions with no central depression ($w=0$) and with a large central depression ($w=1.2$).

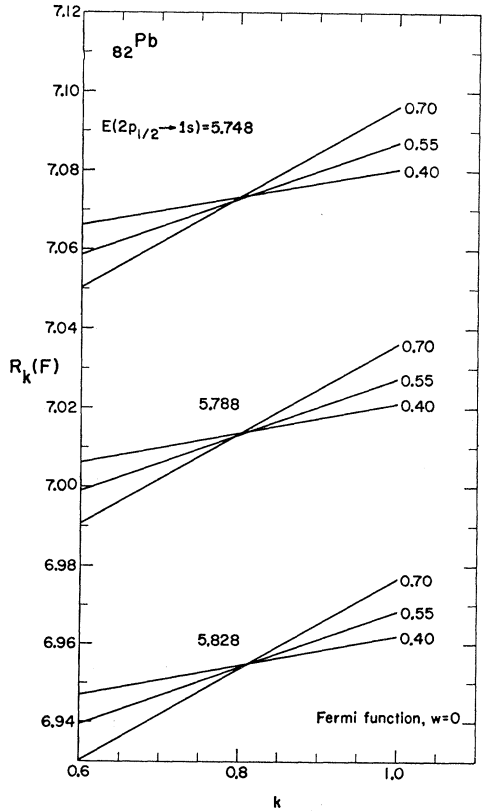

FIG. 9. Graphical determination of energy dependence coefficient C for the $2p_{1/2}\rightarrow 1s_{1/2}$ transition in lead. The equivalent radius R_k varies linearly and the critical k value varies negligibly over the range of energy variation shown.

TABLE VII. Coefficients needed to relate equivalent radii to measured energy difference in Pb^{206}.

Quantum Nos.	Standard energy $E^{(0)}$ (MeV)	Fermi model, $w=0$ k	$R_k^{(0)}$ (F)	C (F/MeV)	Fermi model, $w=1.2$ k	$R_k^{(0)}$ (F)	C (F/MeV)
$2p_{1/2}\rightarrow 1s_{1/2}$	5.78787	0.80	7.013	1.49	0.81	7.030	1.49
$2p_{3/2}\rightarrow 1s_{1/2}$	5.97529	0.83	7.012	1.41	0.85	7.028	1.41
$2p_{3/2}$-$2p_{1/2}$	0.18514	1.22	7.040	29.4	1.23	7.051	29.4
$3d_{3/2}\rightarrow 2p_{1/2}$	2.64299	2.29	7.109	9.10	2.29	7.114	9.10
$3d_{5/2}\rightarrow 2p_{3/2}$	2.49986	2.75	7.150	13.2	2.78	7.160	13.2
$3d_{3/2}\rightarrow 2p_{3/2}$	2.45702	2.76	7.152	13.3	2.77	7.161	13.3
$3d_{5/2}$-$3d_{3/2}$	0.04338	3.25	6.505	1145	3.27	6.512	1145
$4f_{5/2}\rightarrow 3d_{3/2}$	0.97153	4.06	7.351	460	4.10	7.354	460
$4f_{7/2}\rightarrow 3d_{5/2}$	0.93768	4.80	7.739	770	4.82	7.746	725
$3p_{3/2}\rightarrow 2s_{1/2}$	1.50793	0.08	6.983	8.07	0.11	7.021	8.03
$n=\infty\rightarrow 1s_{1/2}$	10.59339	1.03	7.041	1.28	1.03	7.053	1.28

We did this for both the Fermi function with $w=0$ and the Fermi function with $w=1.2$, as a check on model dependence. Results are given in Table VII.

A typical set of results leading to an energy dependence coefficient is shown in Fig. 9. As the assumed $2p_{1/2}\rightarrow 1s_{1/2}$ energy is increased in steps of 0.040 MeV from 5.748 to 5.828 MeV, the equivalent radius R_k decreases by approximately equal steps of 0.060 F from 7.073 F to 6.954 F. At the same time, k changes by about 0.01, which is a negligible change. Note that the horizontal scale of Fig. 9 is expanded relative to the scales of earlier figures.

With the results given in Table VII, any measured energy difference may be converted to an equivalent radius at a particular k value for either of the two models, with the help of Eq. (2). Since the calculations underlying the numbers in Table VII included only the effects of the static nuclear charge distribution and the vacuum-polarization correction, the energy E to be substituted into Eq. (2) is not directly the experimental energy. Rather it is the experimental energy corrected for other estimated effects, such as radiative corrections and nuclear polarization. For the same reason, the uncertainty to be assigned to E must include theoretical uncertainties in these other effects as well as experimental uncertainty. Since the coefficients C in Table VII vary over nearly three orders of magnitude, the uncertainties of equivalent radii deduced from experiment will show a correspondingly great range of variation.

TABLE VIII. Estimated corrections to muonic energy levels in lead.[a]

State	Energies in keV[b] Radiative corrections	Nuclear polarization	Total
$1s_{1/2}$	+2.75(75)	−6.00(100)	−3.25(150)
$2p_{1/2}$	+0.35(20)	−2.10(30)	−1.75(35)
$2p_{3/2}$	+0.65(20)	−1.90(30)	−1.25(35)
$3d_{3/2}$	−0.04(2)	−0.08(4)	−0.12(5)
$3d_{5/2}$	+0.05(2)	−0.08(4)	−0.03(5)
$4f_{5/2}$	−0.01	~0	−0.01
$4f_{7/2}$	+0.01	~0	+0.01
$2s_{1/2}$	+0.70(20)	−0.70(35)	0.00(40)
$3p_{3/2}$	+0.25(7)	−0.10(5)	+0.15(10)

[a] Based primarily on the work of Refs. 10 and 15.
[b] Here a positive sign indicates a repulsive effect, a negative sign an attractive effect.

B. Analysis of Data

If our results were precisely model-independent, the analysis of data would proceed along the following path. (a) To the experimental energies one would apply theoretical corrections to obtain the best estimates of the energy differences E attributable to the static nuclear charge and vacuum polarization. (b) From these energies E one would obtain a set of equivalent radii R_k. (c) One would find out what nuclear charge distributions are compatible with this set of R_k values. All such charge distributions would adequately fit the experimental data. Because of the actual slight model dependence of the results, the procedure cannot be so straightforward. The R_k values deduced from experiment can be strongly suggestive about the form of the charge distribution, and they can indicate what type of variation is possible which does not stray outside the limits of uncertainty. By their smoothness or lack of smoothness, they can also reveal whether *any* spherically symmetric charge distribution is capable of fitting the data. But finally to pin down the parameters of a charge-density function, one must calculate energies and compare them directly with the data. The equivalent radii provide very useful insight and a valuable intermediary between calculations and data, but they are not the last word, at least not when the data are of high accuracy.

We have made no effort to improve on existing estimates of radiative corrections[2,6,10–13] and nuclear polarization corrections.[14,15] The values we have used,

[12] R. C. Barrett, S. J. Brodsky, G. W. Erickson, and M. H. Goldhaber, Phys. Rev. **166**, 1589 (1968).
[13] R. C. Barrett, Phys. Letters **28B**, 93 (1968). This reference came to our attention after our calculations were completed. However, the differences between Barrett's estimates of radiative corrections and those we adopted (Table VIII) are too small to have any effect on our analysis.
[14] R. K. Cole, Jr., Phys. Rev. **177**, 164 (1969).
[15] Min-Yi Chen, Princeton University Technical Report No. PUC-937-291, 1968 (unpublished).

TABLE IX. Energy differences in muonic Pb^{206}.

Quantum Nos.	Experimental energies[a]	Energies in keV: Energies E attributable to static charge plus vacuum polarization	Energies calculated with a Fermi function[b]	Energies calculated with a Bethe-Elton function[c]
$2p_{1/2}\rightarrow 1s_{1/2}$	5788.33(48)	5786.83(160)	5776.89	5785.80
$2p_{3/2}\rightarrow 1s_{1/2}$	5973.88(44)	5971.88(160)	5961.51	5970.72
$2p_{3/2}$-$2p_{1/2}$	185.65(12)	185.15(50)	184.61	184.93
$3d_{3/2}\rightarrow 2p_{1/2}$	2643.75(40)	2642.12(55)	2641.78	2641.38
$3d_{5/2}\rightarrow 2p_{3/2}$	2501.26(36)	2500.04(50)	2499.90	2499.16
$3d_{3/2}\rightarrow 2p_{3/2}$	2457.79(57)	2456.66(65)	2457.16	2456.45
$3d_{5/2}$-$3d_{3/2}$	43.15(10)	43.06(12)	42.73	42.71
$4f_{5/2}\rightarrow 3d_{3/2}$	971.74(20)	971.63(21)	971.78	971.69
$4f_{7/2}\rightarrow 3d_{5/2}$	937.72(20)	937.68(21)	938.22	938.16
$2s_{1/2}\rightarrow 2p_{1/2}$	1217.81(80)	1216.06(100)	1215.16	1212.40
$3p_{3/2}\rightarrow 2s_{1/2}$	1507.93(80)	1507.78(90)	1507.66	1510.07

[a] References 10 and 11.
[b] Parameters: $R/A^{1/3}=1.1290$, $a=0.51$, and $w=0$ ($R_2/A^{1/3}=1.203$).
[c] Parameters: $R/A^{1/3}=1.1219$, $a=1.4$, $\gamma=1.4$, and $w=1.2$ ($R_2/A^{1/3}=1.203$).

together with our estimated uncertainties, are shown in Table VIII. We have regarded the work in Refs. 10 and 15 as most reliable.[12] In Table IX are given the experimental energies of Anderson *et al.*[10,11] and, derived from these, the energy differences E attributable to the static nuclear charge distribution plus vacuum-polarization corrections. Finally, from the data of Tables VII and IX, the equivalent radii are calculated for each of the two models studied in detail. Results are given in Table X and in Figs. 10 and 11. The uncertainties assigned to R_k values in Table X are those based on the energy uncertainties in Table IX, and do not include the further uncertainty associated with model dependence. This is true also of the error bars in Figs. 10 and 11. The numbers in parenthesis in these figures give the energy uncertainties in keV.

Inspection of the seven points with relatively small error bars in Figs. 10 and 11 at once reveals several facts. (1) A single charge distribution can in principle fit all the data, since a simple smooth curve can be drawn through the points. (2) The points define an upward sloping curve, as expected for finite surface thickness. The slope of the curve should provide information on surface thickness. (3) The points suggest a curve of positive curvature, the kind of curve associated with a central depression in the charge-density function. For self-consistency, efforts to fit the data with a function having little or no central depression should make use of Fig. 10. Efforts to fit the data with a function having a large central depression should make use of Fig. 11. Calculations of equivalent radii for intermediate models could be compared with points interpolated between Figs. 10 and 11.

As expected from other considerations, the $4f\rightarrow 3d$ transitions and the doublet d splitting do not provide much information, although they do determine moments of relatively large k. From Figs. 10 and 11, it appears that the reported doublet d splitting[11] of 43.15 keV [16] must be too large by about 0.3 keV. A value of about 42.85 keV is required to be consistent with the other data. If the reported value of 43.15 ± 0.10 keV is confirmed by further measurement, this will be a small but important anomaly. A similar consistency argument suggests that the reported $4f_{7/2}\rightarrow 3d_{5/2}$ energy of 937.72 ± 0.20 keV is too small by about 0.5 keV. Some unknown repulsive effect shifting the $3d_{5/2}$ level upward by 0.3 to 0.5 keV would, of course, explain both of these points at once. Experimental error seems a more likely explanation at present.

As shown in Fig. 10, a precision fit to the data with a Fermi function ($w=0$) is impossible. Since the R_k curve for the Fermi function is nearly a straight line over this range of k, this conclusion could be reached without further calculation. No straight line passes through the points in Fig. 10. The R_k curve for a Fermi function which does a good job of fitting all but the $2p\rightarrow 1s$ transitions is shown by the solid line in Fig. 10.

TABLE X. Equivalent radii of nuclear charge distribution in Pb^{206} as determined from experiment.

Energy difference used to determine moment	Analysis with Fermi model, $w=0$ k	R_k	Analysis with Fermi model, $w=1.2$ k	R_k
$2p_{1/2}\rightarrow 1s_{1/2}$	0.80	7.015(2)	0.81	7.032(2)
$2p_{3/2}\rightarrow 1s_{1/2}$	0.83	7.017(2)	0.85	7.033(2)
$2p_{3/2}$-$2p_{1/2}$	1.22	7.040(15)	1.23	7.051(15)
$3d_{3/2}\rightarrow 2p_{1/2}$	2.29	7.117(5)	2.29	7.122(5)
$3d_{5/2}\rightarrow 2p_{3/2}$	2.75	7.148(7)	2.78	7.158(7)
$3d_{3/2}\rightarrow 2p_{3/2}$	2.76	7.157(9)	2.77	7.166(9)
$3d_{5/2}$-$3d_{3/2}$	3.25	6.871(137)	3.27	6.878(137)
$4f_{5/2}\rightarrow 3d_{3/2}$	4.06	7.305(97)	4.10	7.308(97)
$4f_{7/2}\rightarrow 3d_{5/2}$	4.80	7.739(162)	4.82	7.746(152)
$3p_{3/2}\rightarrow 2s_{1/2}$	0.08	6.984(7)	0.11	7.022(7)

[16] This value is determined from the experimental $\Delta d-\Delta f$ value, assuming the theoretically calculated Δf splitting to be correct.

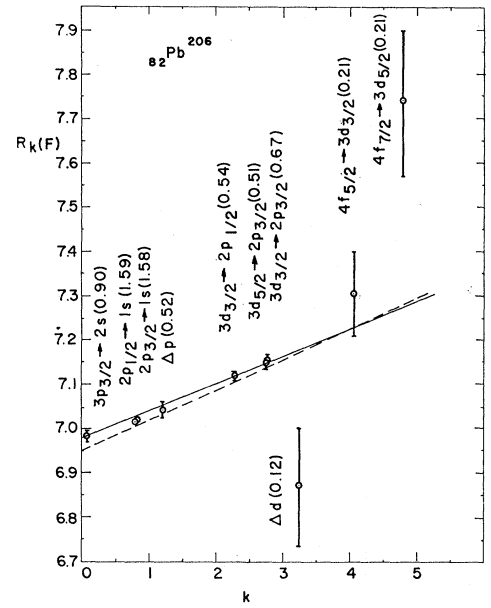

FIG. 10. The points are equivalent radii deduced from experiment (Refs. 10 and 11), using the Fermi function ($w=0$) for analysis. Error bars include theoretical uncertainty in energy corrections. The total energy uncertainties adopted are shown in keV in parentheses. The solid curve is a theoretical curve for the Fermi function whose parameters are given in Table IX. It adequately fits all but the $2p\rightarrow 1s$ energies. The dashed curve is the equivalent-radius curve for a Fermi function which fits electron-scattering data in Pb^{208} (Ref. 17), with radial parameter scaled downward by the factor $(206/208)^{1/3}$.

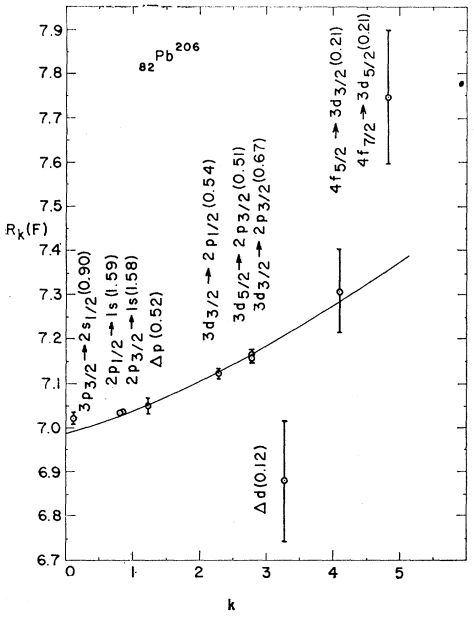

FIG. 11. The points are equivalent radii deduced from experiment (Refs. 10 and 11), using the Fermi function with $w=1.2$ for analysis. The error bars and the numbers in parentheses have the same meaning as in Fig. 10. The curve is a theoretical curve for the Bethe-Elton function whose parameters are given in Table IX. It adequately fits all but the $3p_{3/2}\rightarrow 2s_{1/2}$ and $2s_{1/2}\rightarrow 2p_{1/2}$ transitions.

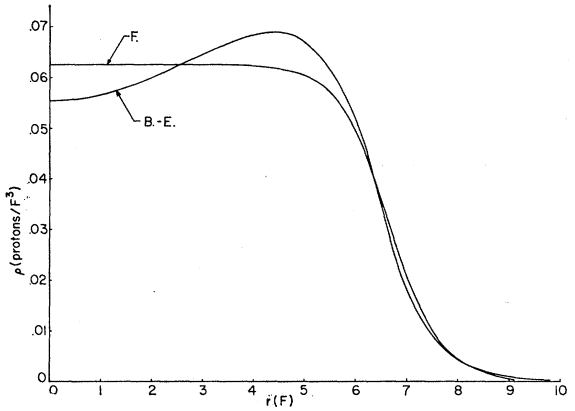

FIG. 12. Charge-distribution functions for Pb^{206}, corresponding to the solid curves in Figs. 10 and 11 and to the calculated energies in Table IX. The labels indicate Fermi and Bethe-Elton functions.

Energies calculated using this function are listed in Table IX. (This is not a least-squares fit.) Also noting that a Fermi function could not accurately fit all the Pb^{206} data, Anderson *et al.*[11] concluded that probably the nuclear polarization effect lowers the $1s$ state by more than the calculated 6 keV. (These authors estimated the extra shift of the $1s$ state *minus* the extra shift of the $2p_{1/2}$ state to be about 7 keV, to be compared with the 4 keV difference shown in Table VIII. Our Fermi fit, Table IX, shows a greater discrepancy, about 10 keV.) Based on our moment analysis, we believed at first that reaching any conclusion about the magnitude of the nuclear polarization effect from an analysis using the Fermi function was quite unjustified, since, with a differently chosen charge-density function, it should be possible to introduce an appropriate curvature into the R_k curve and wipe out the apparent discrepancy. One such effort, unsuccessful, is shown in Fig. 11, with calculated energies listed in Table IX.

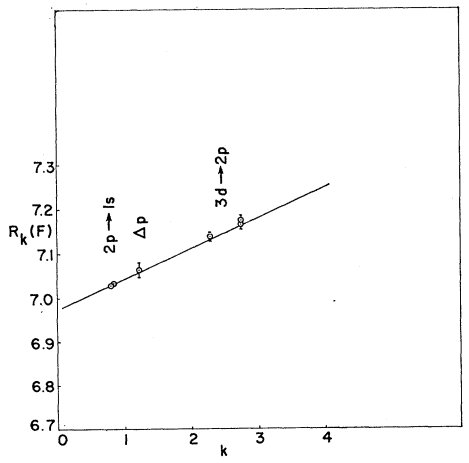

FIG. 13. The points are equivalent radii for Pb^{208} deduced from experiment (Ref. 10), using the Fermi function for analysis. The curve is a theoretical curve using a Fermi function that provides a fit to electron-scattering data for the same isotope (Ref. 17).

TABLE XI. Energy differences in muonic Pb^{208}.

Quantum Nos.	Experimental energies[a]	Energies in keV: Energies E attributable to static charge plus vacuum polarization	Energies in keV: Energies calculated with Fermi function which fits electron scattering data[b]
$2p_{1/2}\rightarrow 1s_{1/2}$	5778.93(50)	5777.43(160)	5778.83
$2p_{3/2}\rightarrow 1s_{1/2}$	5963.67(45)	5961.67(160)	5963.45
$2p_{3/2}$-$2p_{1/2}$	184.84(22)	184.34(55)	184.62
$3d_{3/2}\rightarrow 2p_{1/2}$	2641.48(46)	2639.85(58)	2641.10
$3d_{5/2}\rightarrow 2p_{3/2}$	2499.88(39)	2498.66(52)	2499.20
$3d_{3/2}\rightarrow 2p_{3/2}$	2456.41(59)	2455.28(69)	2456.48
$3d_{5/2}$-$3d_{3/2}$	43.15(10)	43.06(12)	42.72
$4f_{5/2}\rightarrow 3d_{3/2}$	971.74(20)	971.63(21)	971.75
$4f_{7/2}\rightarrow 3d_{5/2}$	937.72(20)	937.68(21)	938.20

[a] Reference 10.

[b] $R/A^{1/3}=1.1186$, $a=0.5348$ ($R_2/A^{1/3}=1.196$); from Ref. 17.

In fact, even with the four-parameter Bethe-Elton function, we have not succeeded in getting a precision fit to all the data. However, the Bethe-Elton function is unwieldy, and perhaps we have not tried hard enough.

We find, in agreement with Anderson *et al.*,[10,11] that it is easy to fit all but the $3p_{3/2}\rightarrow 2s_{1/2}$ and $2s_{1/2}\rightarrow 2p_{1/2}$ energies or all but the $2p\rightarrow 1s$ energies. The data suggest that the actual binding of the $1s$ state is greater than calculated or the actual binding of the $2s$ state is less than calculated. The magnitudes of these possible discrepancies can only be stated roughly as several keV, or, for the $1s$ state, possibly as large as 10 keV. In terms of Fig. 10, this conclusion is that the plotted point at $k\cong 0.10$ is slightly too high, or the plotted points at $k\cong 0.80$ are slightly too low. Changing either would produce a smoother equivalent-radius curve of less curvature. Shown in Fig. 12 are the charge-density functions corresponding to the equivalent radius curves of Figs. 10 and 11 and the calculated energies in Table IX.

The parameters of our Fermi function for Pb^{206} (Table IX) differ somewhat from those in Ref. 11. Our mean-square-radius parameter is $R_2/A^{1/3}=1.203$ F; theirs (called r_0) is 1.199 F. Our surface-thickness parameter is $a=0.51$ ($t=2.24$); theirs is $a=0.47$ ($t=2.05$). The differences are greater than their estimated uncertainties. We attribute these differences not to numerical error in either calculation, but to a different approach in analyzing the data. We pay no heed to the doublet d splitting, since it is inconsistent with the other data, and we include all three $3d\rightarrow 2p$ points in our analysis, whereas they include the doublet d splitting and consider only one of the $3d\rightarrow 2p$ energies. In this way, they are led to a charge-density function whose equivalent-radius curve has lesser slope (smaller a or t) and smaller value of R_2 than the solid curve in Fig. 10.

An important question in such analysis is the consistency of muonic-atom data and electron-scattering data. Figure 13 and Table XI provide some evidence on this point. Ravenhall[17] finds a satisfactory fit to electron-scattering data for Pb^{208}, using a Fermi function with parameters $R/A^{1/3}=1.119$ and $a=0.535$ ($t=2.35$). His parameters, without alteration, provide good agreement[18] with the muonic atom data for Pb^{208}. However, transitions including the $2s$ state in Pb^{208} have not yet been observed. Such transitions will be quite important in testing the consistency of muonic-atom data and electron-scattering data. For the present, the consistency is satisfactory.

As a matter of interest, we also show by a dashed line in Fig. 10 the equivalent-radius curve for Ravenhall's parameters [with R scaled downward by $(206/208)^{1/3}$]. Comparison of the dashed line in Fig. 10 and the solid line in Fig. 13 shows that a simple $A^{1/3}$ law for radius with no change in surface thickness is not adequate to account for the isotopic difference of Pb^{206} and Pb^{208}.

Finally, we remark that the conclusion of Barrett *et al.*[12] that muonic x-ray energies in lead provide evidence for a proton halo is not valid. Even with the data of Ref. 10, which are more accurate than were the data available to Barrett *et al.*, no definite conclusion about a long nebulous tail of the charge distribution can be reached. In order to see the higher moments ($k=4$ to 5) with sufficient accuracy to reach a conclusion, measurements of the $4f\rightarrow 3d$ transition energies to an absolute accuracy of about 0.1 keV or better would be required.

ACKNOWLEDGMENT

We are indebted to Herbert Anderson for making data available to us before publication. One of us (KWF) profited greatly from numerous discussions with Professor Anderson in the summer of 1968.

[17] D. G. Ravenhall (private communication). We are indebted to Dr. Ravenhall for providing this information prior to publication.

[18] Slight alteration of Ravenhall's parameters would provide an even better fit. Improvement would be obtained by increasing the radial parameter by less than 0.1% and by increasing the surface thickness parameter by a few percent.